

ECM-OPCC: Efficient Context Model for Octree-based Point Cloud Compression

Yiqi Jin^{1,2*}, Ziyu Zhu³, Tongda Xu¹, Yuhuan Lin^{1,2}, Yan Wang^{1†}

¹Institute for AI Industry Research (AIR), Tsinghua University

²Department of Automation, Tsinghua University

³Department of Computer Science, Tsinghua University

Abstract

Recently, deep learning methods have shown promising results in point cloud compression. For octree-based point cloud compression, previous works show that the information of ancestor nodes and sibling nodes are equally important for predicting current node. However, those works either adopt insufficient context or bring intolerable decoding complexity (e.g. $> 900s$). To address this problem, we propose a sufficient yet efficient context model and design an efficient deep learning codec for point clouds. Specifically, we first propose a segment-constrained multi-group coding strategy to exploit the autoregressive context while maintaining decoding efficiency. Then, we propose a dual transformer architecture to utilize the dependency of current node on its ancestors and siblings. We also propose a random-masking pre-train method to enhance our model. Experimental results show that our approach achieves state-of-the-art performance for both lossy and lossless point cloud compression. Moreover, our multi-group coding strategy saves 98% decoding time compared with previous octree-based SOTA compression method [8].

1. Introduction

Recently, Deep Point Cloud Compression (DPCC) has outperformed traditional hand-crafted codec [8]. Inspired by learned image compression and traditional point cloud codec, deep learning community invents tree-based, voxel-based, projection-based and point-based compression algorithms: Tree-based approach represents point cloud by octree [15] and aggregates ancestor and sibling information to predict current node occupancy; Voxel-based approach quantizes point cloud into voxel grid [26] and uses

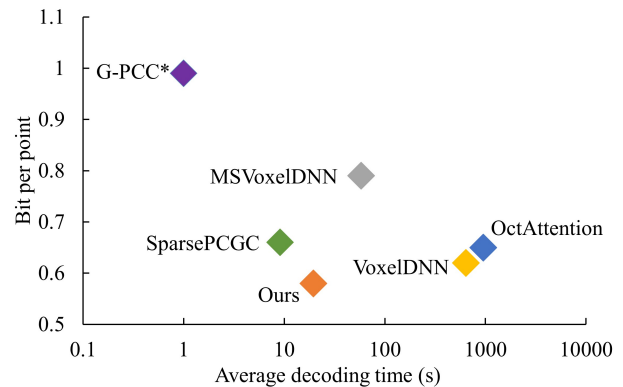


Figure 1. The bpp-decoding time of different methods. Our method achieves SOTA bpp while shows faster or comparable decoding time compared with other deep learning methods. *G-PCC is traditional non-deep learning method.

3D convolution as learned transform; Projection-based approach [29] projects 3D point cloud to 2D image and uses image compression techniques to compress it; And point-based approach [33] utilizes modules from point cloud understanding [19] to transform point cloud and compress transformed points and features. Among above-mentioned methods, octree-based approach is commonly used for large scale sparse point cloud [3].

A major issue of octree-based methods is the decoding complexity due to the autoregressive context model. For example, in [8], both ancestor and sibling information are introduced as autoregressive context models, which greatly increases the decoding complexity. Inspired by parallel autoregressive density estimation [27], we propose to solve this problem by multi-group coding strategy. Specifically, we factorize the fully autoregressive context of [8] into layer-wise autoregressive context, and slice the nodes within the same layers into parallel-decodable context segment. Within each context segment, we deploy group-wise autoregressive context. We propose a dual transformer ar-

*This work is done when Yiqi Jin and Yuhuan Lin are interns at AIR, Tsinghua University

†Yan Wang is the corresponding author.

chitecture to process branches containing ancestor and sibling information. Besides, we introduce random masking pre-training strategy to boost the performance. Experimental results show our method outperforms previous deep point cloud compression methods regarding compression ratio and obtains very competitive decoding speed (Fig. 1).

Our main contributions are as follows:

- We propose a new segment-constrained multi-group coding strategy that enables parallel decoding of nodes inside each group, which greatly accelerates decoding process while maintaining compression performance.
- We propose a novel dual transformer architecture with level-parallel and group-parallel branch to better extract context information from ancestors and siblings.
- We introduce randomly masking input occupancy code as an efficient pre-training strategy to boost performance of our context model.
- Our proposed model achieves SOTA bitrate for lossless compression and R-D (Rate-Distortion) performance for lossy compression. Moreover, it saves 98% decoding time compared with previous work [8].

2. Related Work

2.1. Learned Point Cloud Compression

Voxel-based approaches [24, 25] quantize point cloud to voxel grids and use 3D auto-encoders to compress them. VoxeldNN [21, 22, 23] introduces hybrid compression by first building octree to store structural information of point cloud and then compressing local voxelized point cloud by 3D convolution. Another line of research [31, 30] also uses hybrid scheme but downsamples point cloud by learned-transform first and then utilizes tree-based approach to compress point cloud.

For sparse point cloud, projection based approaches [29, 28, 7, 34] first project point cloud to image then use image compression methods to compress them. [35, 32] directly compress the range images of LiDAR data to leverage the lidar scanning pattern. This kind of method handles large sparse point cloud well and evolves as image compression methods improve. The above mentioned point cloud compression methods can compress point cloud in lossy and lossless way but do not preserve density in different regions of a point cloud. To tackle this problem, point-based methods [33, 13, 16, 19] utilize network designed for raw point cloud segmentation as transform and encode transformed points and features by arithmetic coding.

2.2. Octree-based Point Cloud Compression

Octree-based approaches [15, 2] represent point cloud by octree data structure and convert point cloud compression

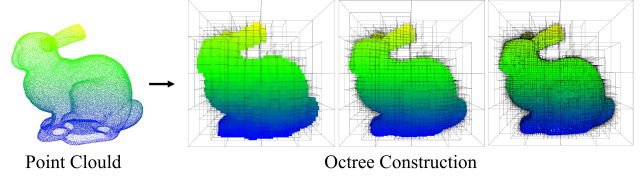


Figure 2. Point cloud BunnyMesh converted to octree with max depth of 5, 6, 7. The accuracy increases with the depth of octree.

to lossless tree structure compression. Specifically, Oct-Squeeze [15] uses deep recurrent model to aggregate ancestral information inside octree to predict occupancy of children node. MuSCLE [2] improves this work by introducing temporal information and traverses octree from both top and bottom for better compression ratio. VoxelContext-Net [26] extracts voxel representation and utilizes 3D convolution based deep entropy model to compress nodes in octree. To further increase receptive field, OctAttention [8] gathers information from sibling and ancestor nodes in a fully autoregressive manner, and introduces attention mechanism for point cloud compression. Aside from the performance enhancement by this fully autoregressive model, the decoding complexity is greatly increased. [5] fit quadratic surfaces with a voxel-based geometry-aware module to provide geometric priors in entropy encoding.

2.3. Efficient Context Model

As we stated above, the autoregressive context in octree-based DPCC greatly increases the decoding complexity (> 900 s per point cloud), which hinders the practical deployment of such methods. On the other hand, advancements in parallelizable autoregressive model in density estimation [27] and language models [10, 9] provide valuable insight for efficient context modeling in deep data compression. In the field of deep image compression, several works try to reduce decoding time by smartly design parallelizable autoregressive context model. Checkerboard context model [12] decodes half latent codes first and uses them as context for the other half. This idea is later adopted in deep video compression for fast decoding [18]. ELIC [11] further improves channel context model by unevenly grouping. However, efficient parallelizable autoregressive context for DPCC is under-explored, which requires considering the uniqueness of point cloud data.

3. Methodology

3.1. Background: Octree-based Compression

Octree is a common data structure to describe 3D space [15]. Each node of octree represents a cube in space. And each node can have eight cubic children that subdivide this node into eight trigrams. The occupancy code of a node is a binary flag to indicate spatial occupancy. An octree can be

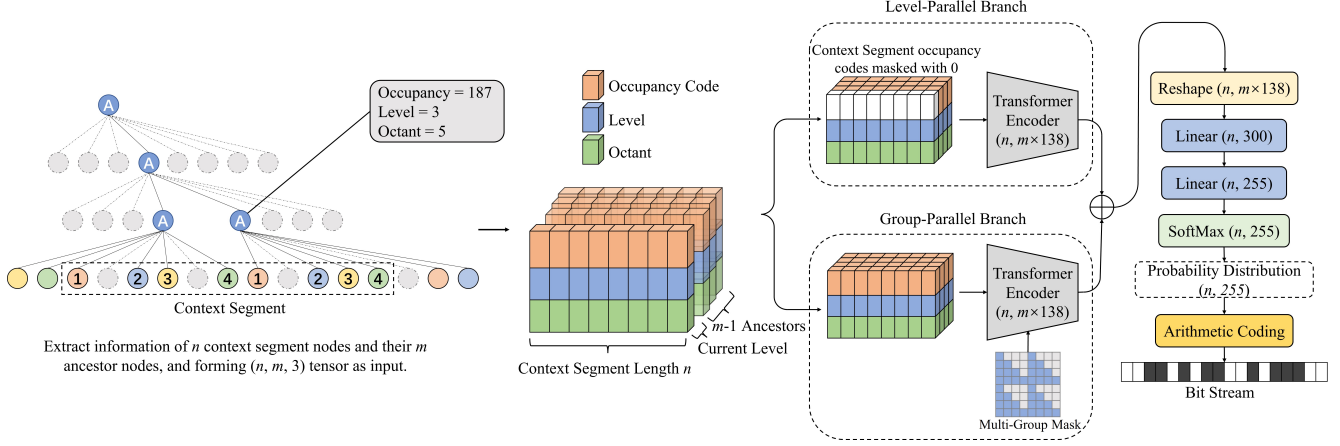


Figure 3. The overall architecture of ECM-OPCC.

represented as the occupancy code sequence of every node. Formally, denote the occupancy code sequence of the whole octree as X , we have

$$X = \{\mathbf{x}^1, \dots, \mathbf{x}^l\} \quad (1)$$

where l is the total level of octree, and \mathbf{x}^i is the occupancy code of level i . The sequence of occupancy codes $\{\mathbf{x}^1, \dots, \mathbf{x}^l\}$ could be used to reconstruct the octree losslessly. The essence of octree-based DPCC is to losslessly compress X . To achieve this, we use a model parameterized by θ to construct a parametric probability distribution $P_\theta(X)$ to approximate the true density $P(X)$. The smaller the KL divergence between the true density $P(X)$ and the predicted probability $P_\theta(X)$ is, the smaller the actual compressed bitrate $\mathbb{E}_{P(X)}[-\log P_\theta(X)]$ we can achieve. Thus, our optimization for bitrate is Eq. 2.

$$\theta^* \leftarrow \arg \min_{\theta} \mathbb{E}_{P(X)}[-\log P_\theta(X)] \quad (2)$$

The distortion of octree-based DPCC only comes from the conversion between octree and point cloud. During the construction of an octree with depth l , a point c_i in raw point cloud C is quantized into the nearest octree cube. While reconstructing octree back to point cloud \hat{C} , the coordinate of c_i is dequantized as the center of cube \hat{c}_i , which brings quantization error e . More specifically, e is bounded as Eq. 3, where w is the max length of leaf cubes, which is determined by l . A deeper octree indicates finer subdivision up to arbitrary precision (See Fig. 2) to achieve lossless compression.

$$e = \max_i \|\hat{c}_i - c_i\|_\infty \leq \frac{w}{2} \quad (3)$$

Naïvely constructing the density of $P_\theta(X)$ as a joint distribution is obviously intractable due to the extremely high dimension of X . Therefore, the key to octree compression

is to construct a tractable factorization to $P_\theta(X)$ by utilizing the domain knowledge of dependency. One possible factorization is the layer-wise autoregressive method:

$$P_\theta(X) = P_\theta(\mathbf{x}^1) \prod_{i=2}^l P_\theta(\mathbf{x}^i | \mathbf{x}^{<i}) \quad (4)$$

Without breaking this layer-wise factorization, we can further use node level and octant as auxiliary information to aid the prediction of occupancy codes. These auxiliary information in current level i can be obtained from the occupancy code of previous level $i-1$. Formally, denote the auxiliary information of level i as \mathbf{y}^i , we have $\mathbf{y}^i = f(\mathbf{x}^{i-1})$. And the auxiliary information can be used to aid the layer-wise autoregressive model as Eq. 5:

$$P_\theta(X) = P_\theta(\mathbf{x}^1) \prod_{i=2}^l P_\theta(\mathbf{x}^i | \mathbf{x}^{<i}, \mathbf{y}^{<i}) \quad (5)$$

Eq. 5 is a more general formulation for OctSqueeze [15], where the conditional relationship on previous layers is limited within the ancestor set of current node and constrained by ancestor order, instead of the whole $\mathbf{x}^{<i}$. Note that these constraints do not affect the asymptotic serial decoding complexity, thus OctSqueeze [15] is a layer-wise factorization method in nature. This layer-wise factorization is very efficient as only information from previous layer is used as context, node within each layer can be decoded in parallel.

To fully exploit the context of ancestors and siblings, one can also adopt node-wise autoregression inside each layer \mathbf{x}^i to obtain a probabilistic model as Eq. 6, where N^i is the length of node in layer i , \mathbf{x}_j^i is the j^{th} node in i^{th} layer. And we call this type of model as fully autoregressive model.

$$P_\theta(\mathbf{x}^i | \mathbf{x}^{<i}, \mathbf{y}^{\leq i}) = P_\theta(\mathbf{x}_1^i | \mathbf{x}^{<i}, \mathbf{y}^{\leq i}) \prod_{j=2}^{N^i} P_\theta(\mathbf{x}_j^i | \mathbf{x}_{<j}^i, \mathbf{x}^{<i}, \mathbf{y}^{\leq i}) \quad (6)$$

In fact, the factorization described by Eq. 6 corresponds to a more general formulation for OctAttention [8], where the conditional relationship is additionally constrained by context window and ancestor order. Note that these constraints do not affect the asymptotic serial decoding complexity, thus OctAttention [8] is a fully autoregressive method in nature. OctAttention achieves SOTA compression performance due to its thorough capture of context information from both ancestors and siblings. However, the decoding of such model is fully sequential. In other words, the decoding time is proportional to $\Theta(\sum_i^l N^i)$, which can be extremely slow ($> 900s$ per point cloud).

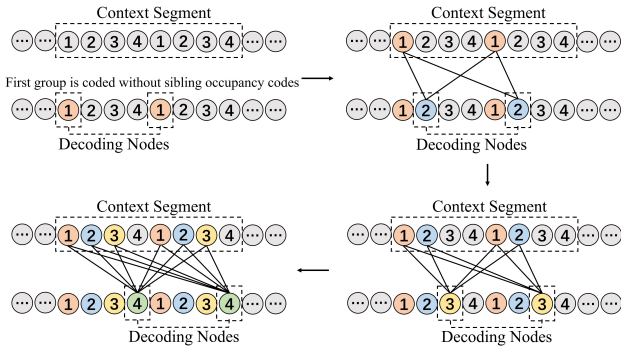


Figure 4. The decoding procedure of 4-group context segment. Nodes within same group (marked with same ID) is decoded in parallel using nodes from previous groups as context.

3.2. Multi-Group Coding Strategy

As stated in Sec. 1, we propose a multi-group coding strategy to support large-scale context while greatly improve coding efficiency over fully autoregressive model [8]. Specifically, we compress layer i of octree autoregressively, with occupancy code $\mathbf{x}^{<i}$, level and octant $\mathbf{y}^{\leq i}$ from previous layers as context. Inside each layer, we divide the nodes into grouped context segment. Then we autoregressively encode each group of nodes, with previous groups inside the context segment as context (Fig. 4). Note that our context segment is different from the context window in OctAttention [8]. Our context segment divides the node in each layer into several parallel decoding segment, while context window in OctAttention is only used to reduce the range of attention calculation and there is no parallelism among different windows.

The previous layer context (ancestor) and same layer context (siblings) are modeled by our dual transformer architecture (Sec. 3.3) to estimate the likelihood for entropy coding. In this way, the decoding process between each context segment and within each group is parallelizable, which greatly reduces decoding complexity. On the other hand, sufficient autoregressive modeling is maintained to promise compression performance.

Formally, denote the j^{th} segment of nodes in layer i as $\mathbf{x}_{w_j}^i = \{\mathbf{x}_{w_j^1}^i, \dots, \mathbf{x}_{w_j^g}^i\}$, where g is the number of group, n is the segment size, h^i is the number of segment in i^{th} layer. Then $\mathbf{x}_{w_j^k}^i$ is the k^{th} group nodes of j^{th} segment in i^{th} layer, and we have the following factorization of layer-wise density:

$$P_\theta(\mathbf{x}^i | \mathbf{x}^{<i}, \mathbf{y}^{\leq i}) = \prod_{j=1}^{h^i} P_\theta(\mathbf{x}_{w_j}^i | \mathbf{x}^{<i}, \mathbf{y}^{\leq i}) \quad (7)$$

$$P_\theta(\mathbf{x}_{w_j}^i | \mathbf{x}^{<i}, \mathbf{y}^{\leq i}) = P_\theta(\mathbf{x}_{w_j^1}^i | \mathbf{x}^{<i}, \mathbf{y}^{\leq i}) \prod_{k=2}^g P_\theta(\mathbf{x}_{w_j^k}^i | \mathbf{x}_{w_j^{<k}}^i, \mathbf{x}^{<i}, \mathbf{y}^{\leq i}) \quad (8)$$

And taking Eq. 7 and Eq. 8 back to the layer-wise autoregressive Eq. 5, we obtain the full likelihood model $P_\theta(X)$. To understand our design choice, we will discuss two questions:

- How multi-group coding affects decoding time?
- How multi-group coding affects the bitrate?

For the first question, let's assume that our hardware is fully parallelizable (e.g. infinitely number of kernels running at the same time). For fully autoregressive model like OctAttention [8], the decoding complexity is $\Theta(\sum_i^l N^i) = \Theta(|X|)$, where $|X|$ is the number of nodes in the octree. For our multi-group coding strategy, we have autoregressive dependency between layers. But for each context segment inside each layer, the decoding is parallelizable. Moreover, although the decoding between groups inside context segment is sequential, for nodes inside each group, the decoding is also parallelizable. Thus, the decoding complexity is greatly reduced to $\Theta(l \cdot g)$. And empirically, as shown in Tab. 1, we also find our decoding time is greatly reduced over OctAttention [8].

For the second question, we can derive the theoretical bitrate as $\mathbb{E}_{P(X)}[-\log P(X)] + D_{KL}[P(X) || \hat{P}_\theta(X)]$ (See details in Appendix). And by applying the conclusion in [14], we have the theoretical lowerbound on the bitrate as Tab. 2. Although the theoretical bitrate lowerbound of our

method is higher than fully autoregressive method, in practice we can achieve better bitrate than OctAttention [8] by smartly design the model (See Sec. 3.3) and optimization (See Sec. 3.4).

	Asymptotic	Practical
fully autoregressive	$\Theta(\sum_{i=1}^l N^i)$	948s
Ours	$\Theta(lg)$	19.5s

Table 1. Asymptotic and practical decoding complexity between fully autoregressive model and our proposed multi-group coding strategy assuming fully parallelizable hardware.

	Theoretical Lowerbound	Practical
fully autoregressive	$\mathbb{E}[-\log P(X)]$	0.65 bpp
Ours	$\mathbb{E}[-\log P(X)] + \sum_{i,j} \mathbb{H}(\mathbf{x}_{w_j}^i \mathbf{x}^{<i}) - \mathbb{H}(X)$	0.58 bpp

Table 2. Theoretical bitrate lowerbound and practical bitrate of fully autoregressive model and our proposed multi-group coding strategy.

3.3. Dual Transformer Structure

We design a novel dual branch transformer structure to support our coding strategy. Despite that our approach is fully autoregressive in layer level in nature, in practice we trace back to at most $m - 1$ ancestors to save calculation (which does not affect the asymptotic complexity discussed above), where m is a hyper-parameter. For each context segment $\mathbf{x}_{w_j}^i$ in layer i , we trace back $m - 1$ ancestor nodes

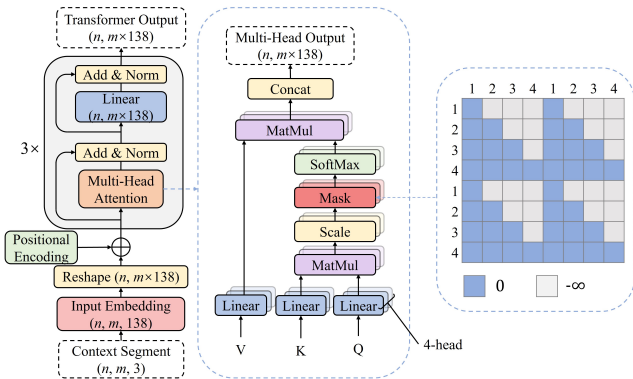


Figure 5. Transformer structure and multi-group mask matrix used in group-parallel branch. The network structure follows OctAttention [8]. In this figure, the length of context segment $n = 8$ and the group count $g = 4$. The blue blocks is 0 and gray blocks is $-\infty$.

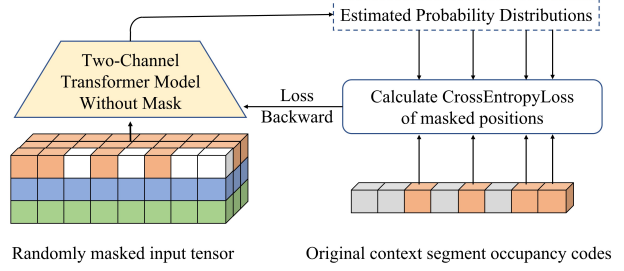


Figure 6. Overview of our pre-train strategy. We use same model without mask to process input, and only backward the loss at masked positions.

for each context segment node (pad zero if not enough), to get $n \times m$ of sibling and ancestor nodes in total. We use occupancy code \mathbf{x} , level and octant \mathbf{y} as context to construct a $n \times m \times 3$ tensor as the input of transformer.

The level-parallel branch is designed to fully use all available information under the requirement that nodes in each level can be encoded and decoded in parallel, corresponding to Eq. 5. As shown in Fig. 3, the occupancy codes of current encoding/decoding level are masked with 0 to prevent information leakage (i.e., only already decoded information can be used for current node). In this branch, the information carried by occupancy code only comes from previous levels, which are ancestor nodes.

The group-parallel branch is designed to exploit context information carried by occupancy code of sibling nodes. As shown in Fig. 5, we use a multi-group mask matrix to modulate the attention layer, which ensures that only already decoded occupancy code from siblings can be used as context for current node. As explained in Fig. 4, nodes in different context segment or nodes in the same group can be encoded or decoded in parallel, corresponding to Eq. 7 and Eq. 8.

For encoding, we just need one forward pass of the two branches to compress all the nodes. For decoding, to decompress the node of each level, we need to run level-parallel branch once, and run group-parallel branch g times, so the total sequential-calculation complexity is $\Theta(l \cdot g)$, as given in Tab. 1.

3.4. Random Masking Pretrain

The essential task of our transformer is to use context $\mathbf{x}^{<i}$, $\mathbf{y}^{<i}$, $\mathbf{x}_{w_j}^{<i}$ to predict current group $\mathbf{x}_{w_j}^i$. Therefore, it is important to fully exploit the predict ability of our transformer-based model. Inspired by BERT [6], we design a pre-train method to help our model develop the ability of predicting current node with context information (Fig. 6). Specifically, we randomly mask the input occupancy code with 50% probability, and use our model (without multi-group mask) to predict the masked positions with unmasked occupancy codes and full information of ancestors. This operation simulates the process of actual coding. As for gradi-

ent backward, we only backward the loss between predicted and ground truth occupancy codes of masked positions.

4. Experiment

4.1. Datasets

We train and test our method on LiDAR and object dataset for comprehensive evaluation.

For LiDAR dataset, we adopt SemanticKITTI [1], which is a large-scale outdoor-scene dataset for sparse point cloud semantic segmentation. It consists of 22 sequences, and contains a total of 43552 scans with 4549 million points.

For Object dataset, we adopt 8i Voxelized Full Bodies (MPEG 8i) [17] and Microsoft Voxelized Upper Bodies (MVUB) [4]. MPEG 8i contains sequences of smooth surface and complete human shape point clouds with 10 and 12bit precision. MVUB contains sequences of five half-body human shape dynamic voxelized point cloud with 9 and 10-bit precision. Due to their fixed precision, MPEG 8i and MVUB are commonly used for lossless compression task to fairly compare the compression rate between different methods.

To ensure fair comparison, we use the same train-test split as previous works [8, 26], and perform lossy compression task on LiDAR dataset, lossless compression task on object datasets.

4.2. Implementation Details

4.2.1 Experimental Setup

All experiments are performed on a machine with NVIDIA A100-PCIE-40GB GPU. We also test our method and OctAttention on the machine with one NVIDIA GeForce RTX 3090 for fair comparison with results reported in SparsePCGC [30]. We use Adam optimizer with $lr = 10^{-3}$. It takes 2-4 days to train our model to 20 epochs. We tried different context segment length n and group number g for ablation study. To balance compression bitrate and decoding time, we set $n = 1024, g = 8$ for LiDAR model and $n = 2048, g = 8$ for object model as default settings.

4.2.2 Baseline Methods

In LiDAR point cloud lossy compression task, we set the maximum level of octree from 8 to 12 to achieve different R-D trade-off. We compare our work with octree-based compression method OctAttention [8], VoxelContext-Net [26] OctSqueeze [15], competitive voxel-based learned method SparsePCGC [30], and traditional hand-crafted G-PCC from MPEG standard in the stable version (TMC13 v14.0) [20]. In object point cloud compression, we set the side length of the leaf cube to 1 to achieve lossless compression. We compare our method with G-PCC, OctAttention, SparsePCGC [30], VoxelDNN [21], MSVoxelDNN

[23]. We apply lossless compression on above methods for fair comparison on bpp and encoding/decoding time.

4.2.3 Training and Testing Strategy

Following previous octree-based works, we train 2 separate model on LiDAR and object datasets. For LiDAR task, we construct the training point cloud to 12-level octree so that our model can learn the distribution at all level in one training procedure. We truncate the octree to 8-12 levels to test our model at different bitrates. For object point clouds, we construct them losslessly to octree for training and testing.

4.2.4 Evaluation Metrics

For fair comparison, we adopt same evaluation metrics with previous works [8, 26]. Specifically, for LiDAR, we use point-to-point (D1 PSNR), point-to-plane (D2 PSNR) and chamfer distance (CD) to measure reconstruction quality in lossy compression. We compare bpp, encoding time and decoding time to evaluate compression performance. The results of compared works are performed on machines with the same GPU configuration. All bpp data are obtained by averaging over sequence.

4.3. Experimental Results

4.3.1 Lossy Compression Performance

The bpp-distortion curves of LiDAR point cloud compression is shown in Fig. 7. Our model outperforms other methods at all bitrates consistently. Specifically, we save 31% bitrate over G-PCC averagely over five distortion levels. We also achieve 8.9% and 4.4% relative reduction at high and low bitrate respectively versus SOTA method OctAttention. Experimental results verify the effectiveness of our multi-group context model over previous methods.

4.3.2 Lossless Compression Performance

The lossless compression results on object datasets are shown in Table 4, our method saves 42.4% and 33.6% bpp averagely on MPEG 8i and MVUB over traditional method G-PCC. We also compare our method w/ and w/o pre-train. Tab. 5 shows that our method w/ pre-train outperforms OctAttention by 6.3% and 1.3% on two datasets, and gets considerable gains over models w/o pre-train.

4.3.3 Encoding and Decoding Efficiency

We adopt MPEG 8i dataset to compare encoding and decoding efficiency. And we compare our results against G-PCC, voxel-based method SparsePCGC [30], VoxelDNN[21], and octree-based method OctAttention [8]. As shown in

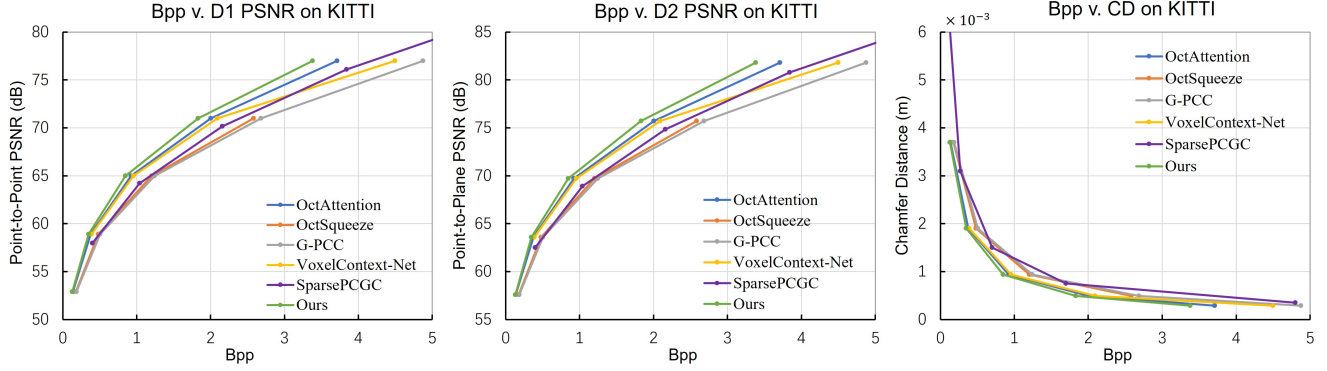


Figure 7. Results of different methods on SemanticKITTI dataset.

Point Cloud	Traditional	Voxel-based		Octree-based	
	G-PCC	SparsePCGC	VoxelDNN	MSVoxelDNN	OctAttention Ours
loot_vox10 (bpp)	0.95	0.63	0.58	0.73	0.62 0.55
redandblack_vox10 (bpp)	1.09	0.72	0.66	0.87	0.73 0.66
boxer_viewdep_vox10 (bpp)	0.94	0.60	0.55	0.70	0.59 0.51
Thaidancer_viewdep_vox10 (bpp)	0.99	0.67	0.68	0.85	0.65 0.58
Average bpp	0.99	0.66	0.62	0.79	0.65 0.58
Average Gain over G-PCC	-	33.8%	37.6%	20.5%	34.6% 41.9%
Average Encoding Time (s)	4.0	9.5	885	54	0.80 1.92
Average Decoding Time (s)	1.0	9.1	640	58	948 19.5

Table 3. Bpp and coding time results on MPEG 8i dataset compared with G-PCC, voxel-based and octree-based methods.

Point Cloud	bpp			Gain*
	G-PCC	OctAttention	Ours	
<i>MPEG 8i</i>				
Loot10	0.95	0.62	0.55	42.1%
Redandblack10	1.09	0.73	0.66	39.4%
Boxer9	0.96	0.60	0.53	45.3%
Boxer10	0.94	0.59	0.51	
Thaidancer9	0.99	0.64	0.59	40.9%
Thaidancer10	0.99	0.65	0.58	
Average	0.99	0.64	0.57	42.4%
<i>MVUB</i>				
Phil9	1.23	0.83	0.79	35.8%
Phil10	1.07	0.79	0.76	29.0%
Ricardo9	1.04	0.79	0.76	34.6%
Ricardo10	1.07	0.72	0.69	35.5%
Average	1.10	0.76	0.73	33.6%

Table 4. Lossless compression results of different methods on MPEG 8i and MVUB datasets. * The bpp saving over G-PCC.

Point Cloud	Ours (w/o pre-train)		Ours (w/ pre-train)	
	bpp	Gain*	bpp	Gain*
MPEG 8i	0.61	4.7%	0.60	6.3%
MVUB	0.77	-1.3%	0.75	1.3%

Table 5. Ablation study of lossless compression on MPEG 8i and MVUB dataset. * The bpp saving over OctAttention.

ods in compression performance, and saves 98% of decoding time compared with Octattention. The encoding time of our method is slower than Octattention due to the dual transformer structure. Moreover, a scatter plot of bpp and decoding time is shown in Fig. 1. It can be seen that our method achieves SOTA compression performance with very fast decoding time.

4.4. Ablation Study and Analysis

4.4.1 Dual Branch Transformer

To explore the effectiveness of our dual branch transformer, we separate the two branches into independent models and test them separately. We adopt MPEG 8i dataset and test

Tab. 3, our method outperforms other deep learning meth-

average bpp, encoding time, total decoding time and neural network inference time to evaluate the performance. We set context segment length $n = 2048$ and group count $g = 8$ for group-parallel branch, we train 20 epochs for each model. Tab. 6 demonstrates that the bitrate results obtained by the separate models are worse than the dual model. Meanwhile, both branches are marginally accelerated in decoding, as the size of neural network is reduced. The level-parallel branch can decode the context segment in parallel, so that the running time of neural network is negligible. Experimental results verify that the dual branch approach is important to compression performance while brings only marginal decoding time overhead.

4.4.2 Effect of Context Segment Length

We set the context segment length $n \in \{128, 256, 512, 1024, 2048, 4096\}$ to study the effect of n . For each model we set group count $g = 8$ and train 20 epochs. And all other parameters remain the same. Tab. 7 shows we obtain 12.1% reduction on bitrate by enlarging n from 128 to 2048, this is because more context information can be used in a larger segment. Moreover, because expanding the context segment size n can reduce the number of forward pass and enable our device to process data continuously, we reduce the encoding time by 7.5 times, and decoding time by 8.4 times. And we also reduce neural network inference time, which decreases by 12 times while decoding. Therefore, enlarging context segment will be more effective and also more efficient in our method. We set $n = 2048$ for best performance under the constrain of GPU memory. We do not implement multi-threading in our paper, the impact of n on efficiency only holds under this condition, and the speedup in Tab. 3 is brought by the reduction of serial decoding complexity.

Branch	Avg. bpp on MPEG 8i	Encoding time (s)	Decoding time (s)	
			Total	Network
Level (L)	0.75	0.79	7.2	0.8
Group (G)	0.64	0.82	9.4	4.0
Dual (L+G)	0.58	1.43	11.7	6.9

Table 6. Independent performance of two branches on object dataset MPEG 8i.

4.4.3 Effect of Group Count

We also study the effect of group count g on the performance of our coding strategy. We set group count $g = \{2, 4, 6, 8, 16, 32\}$, $n = 2048$ and train the model for 20 epochs. Tab. 8 demonstrates that we save 13.6% bitrate by increasing group count from 2 to 32. This is because as

n	Avg. bpp on MPEG 8i	Encoding time (s)	Decoding time (s)	
			Total	Network
128	0.66	10.8	98.8	84.3
256	0.66	5.54	55.0	44.1
512	0.61	2.68	29.9	22.5
1024	0.59	1.46	16.4	11.0
2048	0.58	1.43	11.7	6.9
4096*	-	-	-	-

Table 7. Performance of bpp and coding time on object dataset MPEG 8i when using various context segment length. * We can not provide result with $n = 4096$, as it exceeds 40G GPU memory while training.

g	Avg. bpp on MPEG 8i	Encoding time (s)	Decoding time (s)	
			Total	Network
2	0.66	1.38	7.9	2.6
4	0.61	1.30	8.8	3.6
8	0.58	1.43	11.7	6.9
16	0.57	1.26	19.2	13.6
32	0.57	1.37	33.3	26.6

Table 8. Performance of bpp and coding time on object dataset MPEG 8i when using various group count.

the group count increases, more occupancy codes of sibling nodes can be used as guiding information by latter groups. The encoding time remains similar, as the encoding procedure is always in parallel. Also, because the decoding procedure is sequentially conducted by group, the decoding time shows a multiple upward trend with the increase of group count. It is also noteworthy that when $g \geq 8$, the gain in bpp becomes only marginal while the increment in decoding time becomes significant. We set $g = 8$ as it is a sweet-spot with reasonably good compression performance and fast decoding time.

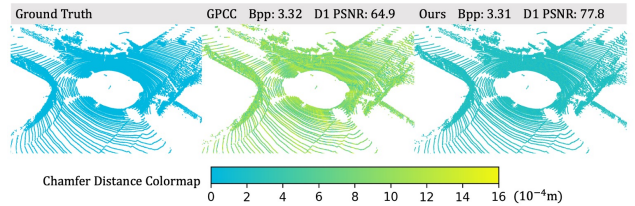


Figure 8. Chamfer distance between normalized ground truth and reconstructed point clouds on SemanticKITTI dataset.

4.5. Qualitative Results

Fig. 8 shows the visualized distortion of our method and G-PCC at similar compression rate. Our method outperforms G-PCC by more than 10 dB on D1 PSNR.

5. Conclusion

In this work, We propose an efficient large-scale context entropy model for point cloud geometry compression. To be specific, we propose a multi-group coding strategy to encode and decode the octree efficiently, based on which we propose a dual transformer architecture. We also design a random masking pre-train strategy. Results show that our model achieves SOTA compression performance, and reduce decoding time by up to 98% compared to previous octree-based works (OctAttention [8]), which makes the practical deployment of octree-based DPCC possible.

References

- [1] Jens Behley, Martin Garbade, Andres Milioto, Jan Quen-
zel, Sven Behnke, Cyrill Stachniss, and Juergen Gall. Se-
mantickitti: A dataset for semantic scene understanding of
lidar sequences. *IEEE/CVF International Conference on
Computer Vision (ICCV)*, page 9296–9306, 2019.
- [2] Sourav Biswas, Jerry Liu, Kelvin Wong, Shenlong Wang,
and Raquel Urtasun. Muscle: Multi sweep compression of
lidar using deep entropy models. In H. Larochelle, M. Ran-
zato, R. Hadsell, M.F. Balcan, and H. Lin, editors, *Advances
in Neural Information Processing Systems*, volume 33, pages
22170–22181. Curran Associates, Inc., 2020.
- [3] Chao Cao, Marius Preda, and Titus Zaharia. 3d point cloud
compression: A survey. In *The 24th International Confer-
ence on 3D Web Technology*, pages 1–9, 2019.
- [4] Loop Charles, Cai Qin, Orts Escolano Sergio, and A. Chou
Philip. Microsoft voxelized upper bodies - a voxelized
point cloud dataset. *ISO/IEC JTC1/SC29 Joint WG11/WG1
(MPEG/JPEG) input document m38673/M7201*, 2016.
- [5] Zhili Chen, Zian Qian, Sukai Wang, and Qifeng Chen. Point
cloud compression with sibling context and surface priors. In
*Computer Vision – ECCV 2022: 17th European Conference,
Tel Aviv, Israel, October 23–27, 2022, Proceedings, Part
XXXVIII*, page 744–759, Berlin, Heidelberg, 2022. Springer-
Verlag.
- [6] Jacob Devlin, Ming-Wei Chang, Kenton Lee, and Kristina
Toutanova. Bert: Pre-training of deep bidirectional trans-
formers for language understanding, 2018.
- [7] Yu Feng, Shaoshan Liu, and Yuhao Zhu. Real-time spatio-
temporal lidar point cloud compression. In *2020 IEEE/RSJ
international conference on intelligent robots and systems
(IROS)*, pages 10766–10773. IEEE, 2020.
- [8] Chunyang Fu, Ge Li, Rui Song, Wei Gao, and Shan Liu. Oc-
tattention: Octree-based large-scale contexts model for point
cloud compression. *arXiv preprint arXiv:2202.06028*, 2022.
- [9] Marjan Ghazvininejad, Omer Levy, Yinhan Liu, and Luke
Zettlemoyer. Mask-predict: Parallel decoding of conditional
masked language models. *arXiv preprint arXiv:1904.09324*,
2019.
- [10] Jiatao Gu, James Bradbury, Caiming Xiong, Victor OK Li,
and Richard Socher. Non-autoregressive neural machine
translation. *arXiv preprint arXiv:1711.02281*, 2017.
- [11] Dailan He, Ziming Yang, Weikun Peng, Rui Ma, Hongwei
Qin, and Yan Wang. Elic: Efficient learned image compres-
sion with unevenly grouped space-channel contextual adap-
tive coding. In *Proceedings of the IEEE/CVF Conference
on Computer Vision and Pattern Recognition*, pages 5718–
5727, 2022.
- [12] Dailan He, Yaoyan Zheng, Baocheng Sun, Yan Wang,
and Hongwei Qin. Checkerboard context model for effi-
cient learned image compression. In *Proceedings of the
IEEE/CVF Conference on Computer Vision and Pattern
Recognition*, pages 14771–14780, 2021.
- [13] Yun He, Xinlin Ren, Danhang Tang, Yinda Zhang, Xi-
angyang Xue, and Yanwei Fu. Density-preserving deep point
cloud compression. In *Proceedings of the IEEE/CVF Con-*

- ference on Computer Vision and Pattern Recognition, pages 2333–2342, 2022.
- [14] Fei Huang, Tianhua Tao, Hao Zhou, Lei Li, and Minlie Huang. On the learning of non-autoregressive transformers. In Kamalika Chaudhuri, Stefanie Jegelka, Le Song, Csaba Szepesvari, Gang Niu, and Sivan Sabato, editors, *Proceedings of the 39th International Conference on Machine Learning*, volume 162 of *Proceedings of Machine Learning Research*, pages 9356–9376. PMLR, 17–23 Jul 2022.
 - [15] Lila Huang, Shenlong Wang, Kelvin Wong, Jerry Liu, and Raquel Urtasun. Octsqueeze: Octree-structured entropy model for lidar compression. In *Proceedings of the IEEE/CVF Conference on Computer Vision and Pattern Recognition (CVPR)*, June 2020.
 - [16] Tianxin Huang and Yong Liu. 3d point cloud geometry compression on deep learning. In *Proceedings of the 27th ACM international conference on multimedia*, pages 890–898, 2019.
 - [17] Ryan Killea, Yun Li, Saeed Bastani, and Paul McLachlan. 8i voxelized full bodies - a voxelized point cloud dataset. *ISO/IEC JTC1/SC29 Joint WG11/WG1 (MPEG/JPEG) input document WG11M40059/WG1M74006*, 2017.
 - [18] Jiahao Li, Bin Li, and Yan Lu. Hybrid spatial-temporal entropy modelling for neural video compression. *arXiv preprint arXiv:2207.05894*, 2022.
 - [19] Zujie Liang and Fan Liang. Transpcc: Towards deep point cloud compression via transformers. 2022.
 - [20] MPEG. <https://github.com/MPEGGroup/mpeg-pcc-tmc13>, 2021.
 - [21] Dat Thanh Nguyen, Maurice Quach, Giuseppe Valenzise, and Pierre Duhamel. Learning-based lossless compression of 3d point cloud geometry. In *ICASSP 2021-2021 IEEE International Conference on Acoustics, Speech and Signal Processing (ICASSP)*, pages 4220–4224. IEEE, 2021.
 - [22] Dat Thanh Nguyen, Maurice Quach, Giuseppe Valenzise, and Pierre Duhamel. Lossless coding of point cloud geometry using a deep generative model. *IEEE Transactions on Circuits and Systems for Video Technology*, 31(12):4617–4629, 2021.
 - [23] Dat Thanh Nguyen, Maurice Quach, Giuseppe Valenzise, and Pierre Duhamel. Multiscale deep context modeling for lossless point cloud geometry compression. In *2021 IEEE International Conference on Multimedia & Expo Workshops (ICMEW)*, pages 1–6. IEEE, 2021.
 - [24] Maurice Quach, Giuseppe Valenzise, and Frederic Dufaux. Learning convolutional transforms for lossy point cloud geometry compression. In *2019 IEEE international conference on image processing (ICIP)*, pages 4320–4324. IEEE, 2019.
 - [25] Maurice Quach, Giuseppe Valenzise, and Frederic Dufaux. Improved deep point cloud geometry compression. In *2020 IEEE 22nd International Workshop on Multimedia Signal Processing (MMSP)*, pages 1–6. IEEE, 2020.
 - [26] Zizheng Que, Guo Lu, and Dong Xu. Voxelcontext-net: An octree based framework for point cloud compression. In *Proceedings of the IEEE/CVF Conference on Computer Vision and Pattern Recognition*, pages 6042–6051, 2021.
 - [27] Scott Reed, Aäron van den Oord, Nal Kalchbrenner, Sergio Gómez Colmenarejo, Ziyu Wang, Yutian Chen, Dan Belov, and Nando de Freitas. Parallel multiscale autoregressive density estimation. In Doina Precup and Yee Whye Teh, editors, *Proceedings of the 34th International Conference on Machine Learning*, volume 70 of *Proceedings of Machine Learning Research*, pages 2912–2921. PMLR, 06–11 Aug 2017.
 - [28] Xuebin Sun, Han Ma, Yuxiang Sun, and Ming Liu. A novel point cloud compression algorithm based on clustering. *IEEE Robotics and Automation Letters*, 4(2):2132–2139, 2019.
 - [29] Chenxi Tu, Eijiro Takeuchi, Alexander Carballo, and Kazuya Takeda. Point cloud compression for 3d lidar sensor using recurrent neural network with residual blocks. In *2019 International Conference on Robotics and Automation (ICRA)*, pages 3274–3280. IEEE, 2019.
 - [30] Jianqiang Wang, Dandan Ding, Zhu Li, Xiaoxing Feng, Chuntong Cao, and Zhan Ma. Sparse tensor-based multi-scale representation for point cloud geometry compression. *arXiv preprint arXiv:2111.10633*, 2021.
 - [31] Jianqiang Wang, Dandan Ding, Zhu Li, and Zhan Ma. Multi-scale point cloud geometry compression. In *2021 Data Compression Conference (DCC)*, pages 73–82. IEEE, 2021.
 - [32] Sukai Wang and Ming Liu. Point cloud compression with range image-based entropy model for autonomous driving. In *Computer Vision–ECCV 2022: 17th European Conference, Tel Aviv, Israel, October 23–27, 2022, Proceedings, Part XXII*, pages 323–340. Springer, 2022.
 - [33] Kang You and Pan Gao. Patch-based deep autoencoder for point cloud geometry compression. In *ACM Multimedia Asia*, pages 1–7. 2021.
 - [34] Lili Zhao, Kai-Kuang Ma, Zhili Liu, Qian Yin, and Jianwen Chen. Real-time scene-aware lidar point cloud compression using semantic prior representation. *IEEE Transactions on Circuits and Systems for Video Technology*, 2022.
 - [35] Xuanyu Zhou, Charles R. Qi, Yin Zhou, and Dragomir Anguelov. Riddle: Lidar data compression with range image deep delta encoding, 2022.

Appendix to ECM-OPCC: Efficient Context Model for Octree-based Point Cloud Compression

1. Proof of Bitrate Lowerbound in Sec. 3.2

In this section, we formalize and proof the theoretical claim on the bitrate lowerbound that is informally given in Tab. 2 of Sec 3.2. For clarity, in this section, we omit \mathbf{y}^i from conditioning. As \mathbf{y}^i is fully deterministic given \mathbf{x}^{i-1} , this omission does not impact the lowerbound of bitrate.

Theorem 1. *For fully autoregressive model, the lowerbound of bitrate $R(X)$ to encode X as symbols $\{\mathbf{x}_1^1, \dots, \mathbf{x}_{N^1}^1, \dots, \mathbf{x}_{N^l}^l\}$ with entropy model $P_\theta(\mathbf{x}_1^1), \dots, P_\theta(\mathbf{x}_{N^1}^1 | \mathbf{x}_{<N^1}^1), \dots, P_\theta(\mathbf{x}_{N^l}^l | \mathbf{x}_{<N^l}^l)$ is $\lceil \mathbb{E}[-\log P(X)] \rceil$, where $\lceil \cdot \rceil$ is the upper rounding operator. This bound is achievable given perfect parameter estimation and the entropy model family covers original distribution.*

Proof. From optimal source coding lowerbound [1], we have $\mathbb{E}_P[-\log P_\theta(X)] \leq R(X)$, and $P_\theta(X) = P_\theta(\mathbf{x}_1^1) \prod P_\theta(\mathbf{x}_j^i | \mathbf{x}_{<^i}^i, \mathbf{x}_{<^j}^j)$. Then we have

$$\begin{aligned} & \mathbb{E}_P[-\log P_\theta(X)] \\ &= \mathbb{E}_P[-\log P(X)] + D_{KL}[P(X) || P_\theta(X)] \\ &\geq \mathbb{E}_P[-\log P(X)] \end{aligned} \quad (9)$$

, and the equality holds only when $D_{KL}[P(X) || P_\theta(X)] = 0$. In other words, when $P(X) = P_\theta(X)$, this lowerbound is achievable. \square

Theorem 2. *For the proposed window-wise parallel autoregressive model, the lowerbound of bitrate to encode X as symbols $\{\mathbf{x}_{w_1}^1, \dots, \mathbf{x}_{w_{h_1}}^1, \dots, \mathbf{x}_{w_{h_l}}^l\}$ with entropy model $P_\theta(\mathbf{x}_{w_1}^1), \dots, P_\theta(\mathbf{x}_{w_{h_1}}^1), \dots, P_\theta(\mathbf{x}_{w_{h_l}}^l | \mathbf{x}_{<^l}^l, \mathbf{x}_{w_{<h_l}^l}^l)$ is $\lceil \mathbb{E}[-\log P(X)] \rceil + \sum_{ij} \mathbb{H}(\mathbf{x}_{w_j}^i | \mathbf{x}_{<^i}^i) - \mathbb{H}(X)$, where $\lceil \cdot \rceil$ is the upper rounding operator and \mathbb{H} is the entropy. This bound is achievable given perfect parameter estimation, the entropy model family covers original distribution, the original distribution factorizes as window size and each group contains only 1 node.*

Proof. As we have

$$\begin{aligned} P_\theta(X) &= P_\theta(\mathbf{x}^1) \prod P_\theta(\mathbf{x}^i | \mathbf{x}^{<i}) \quad (10) \\ P_\theta(\mathbf{x}^i | \mathbf{x}^{<i}) &= P_\theta(\mathbf{x}_{w_1}^i | \mathbf{x}^{<i}) \prod P_\theta(\mathbf{x}_{w_j}^i | \mathbf{x}^{<i}, \mathbf{x}_{w_{<j}}^i) \quad (11) \end{aligned}$$

From [5], we have:

$$\begin{aligned} & D_{KL}[P(\mathbf{x}^i | \mathbf{x}^{<i}) || P_\theta(\mathbf{x}^i | \mathbf{x}^{<i})] \\ &\geq \sum_j \mathbb{H}(\mathbf{x}_{w_j}^i | \mathbf{x}^{<i}) - \mathbb{H}(\mathbf{x}^i | \mathbf{x}^{<i}) \end{aligned} \quad (12)$$

Then from the chain rule of entropy and relative entropy [1], we have:

$$\begin{aligned} & D_{KL}[P(X) || P_\theta(X)] \\ &= \sum_i D_{KL}[P(\mathbf{x}^i | \mathbf{x}^{<i}) || P_\theta(\mathbf{x}^i | \mathbf{x}^{<i})] \\ &\geq \sum_i (\sum_j \mathbb{H}(\mathbf{x}_{w_j}^i | \mathbf{x}^{<i}) - \mathbb{H}(\mathbf{x}^i | \mathbf{x}^{<i})) \\ &= \sum_i \sum_j \mathbb{H}(\mathbf{x}_{w_j}^i | \mathbf{x}^{<i}) - \mathbb{H}(X) \end{aligned} \quad (13)$$

Then, taking Eq. 13 into Eq. 9 and following the proof of Thm. 1 complete the proof. \square

2. More Related Works

In general, there are four types of DPCC frameworks: octree-based, voxel-based, projection-based and point-based approach. Octree-based compression is introduced in the main text. Voxel-based approaches [12] [13] quantize point cloud to voxel grids and use 3D auto-encoders to compress them. VoxelDNN [9, 10, 11] introduces hybrid compression by first building octree to store structural information of point cloud and then compressing local voxelized point cloud by 3D convolution. Another line of research [18, 17] also uses hybrid scheme but downsamples point cloud by learned-transform first and then utilizes tree-based approach to compress point cloud. Without autoregressive context modeling, these methods fail to generalize on sparse point cloud [3]. For sparse point cloud, projection

Distortion			G-PCC	OctSqueeze	VoxelContext-net	OctAttention	Ours	Gain*
D1 PSNR	D2 PSNR	CD						
52.9	57.6	0.003700	0.185	0.177	-	0.137	0.131	29.19%
58.9	63.6	0.001900	0.505	0.480	0.390	0.376	0.348	31.12%
65.0	69.7	0.000937	1.245	1.202	0.956	0.924	0.847	31.95%
71.0	75.7	0.000492	2.684	2.582	2.089	2.004	1.831	31.78%
77.0	81.8	0.000290	4.874	-	4.497	3.711	3.380	30.65%

Table 9. Detail results for LiDAR point cloud compression. *The bpp saving over G-PCC

based approaches [16, 15, 2, 20] first project point cloud to image then use image compression methods to compress then. This kind of method handles large sparse point cloud well and evolves as image compression methods improve. The above mentioned point cloud compression methods can compress point cloud in lossy and lossless way but do not preserve density in different regions of a point cloud. To tackle this problem, point-based methods [19, 4, 6, 7] utilize network designed for raw point cloud segmentation as transform and encode transformed points and features by arithmetic coding.

3. More Implementation Details

3.1. Datasets

To make fair comparison, we use the same training sequences as previous works [3, 14]. For object point clouds, we use Soldier10 and Longdress10 sequences in MPEG 8i, Andrew10, David10, Sarah10 sequences in MVUB for training. We select Loot10, Redandblack10, Boxer9, Boxer10, Thaidancer9, Thaidancer10 in MPEG 8i, Phil9, Phil10, Ricardo9, Ricardo10 in MVUB for testing. For LiDAR datasets, we use sequences 00 to 10 (23201 scans in total) for training, and 11 to 21 (20351 scans in total) for testing. All testing sequences were not used in training. Specifically, Boxer9, Boxer10, Thaidancer9, Thaidancer10 are sequences containing only one frame, we repeat the test 20 times and take the average coding time as results to avoid fluctuation.

3.2. Experimental Setup

We intended to perform previous methods G-PCC [8], VoxelDNN [9], MSVoxelDNN [11], SparsePCGC [17] and OctAttention [3] on our machine to make fair comparison on coding performance and efficiency. However, some of the works above do not have open-source code or have not provide standard trained models. Therefore, we use results from SparsePCGC [17], which contains bpp, encoding time and decoing time results of G-PCC, VoxelDNN, MSVoxelDNN and SparsePCGC on loot_vox10, redandblack_vox10, boxer viewdep_vox10 and Thaidancer_viewdep_vox10.

CPU Specifications (s)	8157 (Ours)	6226R
Total Cores	24	16
Processor Base Frequency	2.30 GHz	2.90 GHz

Table 10. CPU specifications of Intel Xeon Platinum 8157 and Intel Xeon 6226R. Data comes from Intel official website.

Point Cloud	Encoding time (s)	Decoding time (s)
longdress_vox10_1300	5.5	3.8
redandblack_vox10_1550	5.0	3.5
soldier_vox10_0690	7.5	5.0
loot_vox10_1200	5.9	4.1
Average	6.0 (*4.0)	4.1 (*1.0)

Table 11. Coding time of G-PCC on four point cloud frames. *The average results reported in SparsePCGC [17].

According to [17], these testings are performed on a machine with Intel Xeon 6226R CPU and a Nvidia GeForce RTX 3090 GPU. Therefore, to make fair comparison, we test our model and OctAttention on a machine with Intel Xeon Platinum 8157 CPU and a Nvidia GeForce RTX 3090 GPU. The comparison between our method and OctAttention is completely reliable. We do the following illustration to show that the comparison between our results and results in SparsePCGC is promising. The only difference on hardware configuration between two machines is CPU. The specifications of two CPUs is shown in Tab. 10. Data show that the computing ability of two CPUs is at same level. To make further confirmation, we test G-PCC (only use CPU to compute) coding time on our machine, the coding time is shown in Tab. 11. Results demonstrate that our machine do not take advantage over CPU computing speed.

We perform our ablation experiments on a machine with AMD EPYC 7742 CPU and NVIDIA A100-PCIE-40GB GPU. The results performed on this machine are only used in ablation analysis to avoid unfair comparison.

Method	Parameter Count	FLOPs
OctAttention	4.2 M	7.77 G
ECM-OPCC	8.0 M	18.09 G

Table 12. Model size (parameter count) and FLOPs (for single forward computation) comparison between our method and OctAttention, the length of input is 1024.

Point Cloud	OctAttention	Ours (w/o pre-train)	Ours (w/ pre-train)
<i>MPEG 8i</i>			
Loot10	0.62	0.59	0.58
Redandblack10	0.73	0.70	0.69
Boxer9	0.60	0.57	0.56
Boxer10	0.59	0.55	0.54
Thaidancer9	0.64	0.64	0.62
Thaidancer10	0.65	0.62	0.61
Average	0.64	0.61	0.60
<i>MVUB</i>			
Phil9	0.83	0.82	0.80
Phil10	0.79	0.80	0.78
Ricardo9	0.72	0.72	0.70
Ricardo10	0.72	0.73	0.72
Average	0.76	0.77	0.75

Table 13. Complete bpp results on w/o pre-train and w/ pre-train models compared against OctAttention

4. More Experimental Results

4.1. Model Size and Computation Cost

Tab. 12 shows the model size and computation cost (FLOPs) of our method and OctAttention. Our model costs more on a single forward computation due to the dual-channel structure, but the time we need to call the model to compress a point cloud is greatly reduced due to our coding strategy.

4.2. Results for lossless compression on LiDAR

We use bpp results from previous works since some of the compared methods do not have open-source code. The bpp results of previous works could be used directly, for bpp results of same method stay the same while conducting on different machines. The complete results are shown in Tab. 9 We draw the data in Tab. 9 as Fig. 7 in the main text.

4.3. Results for Comparison against OctAttention

We set context window length $n = 1024$, and trained our model for 8 epochs to specifically compare with OctAttention, which use above settings. We test w/ and w/o pre-training step to vetify the effectiveness of pre-train method. The complete bpp results are shown in Tab. 13.

Level-Parallel Branch				
Point Cloud	Avg. Bpp on MPEG 8i	Encoding time (s)	Decoding time (s)	
			Total	Network
Loot10	0.72	0.93	7.90	0.92
Redandblack10	0.83	0.86	7.70	0.90
Boxer9	0.71	0.34	3.00	0.37
Boxer10	0.67	1.17	10.90	1.27
Thaidancer	0.81	0.32	2.97	0.37
Thaidancer10	0.75	1.13	10.70	1.23
Average	0.75	0.79	7.20	0.84

Table 14. Level-parallel branch, context window length $n = 2048$, training for 20 epochs.

4.4. Results of Dual Branch Ablation Study

The complete results of separate branches and dual model is shown in Tab. 14 to 16. We set context window length $n = 2048$ for three models, group count $g = 8$ for group-parallel branch and dual model. We train each model in ablation study for 20 epochs.

Group-Parallel Branch				
Point Cloud	Avg. Bpp on MPEG 8i	Encoding time (s)	Decoding time (s)	
			Total	Network
Loot10	0.62	0.96	11.1	4.6
Redandblack10	0.73	0.89	10.3	4.3
Boxer9	0.60	0.35	3.8	1.7
Boxer10	0.59	1.20	14.0	5.9
Thaidancer	0.65	0.33	3.7	1.6
Thaidancer10	0.65	1.17	13.4	5.7
Average	0.64	0.82	9.4	4.0

Table 15. Group-parallel branch, context window length $n = 2048$, group count $g = 8$, training for 20 epochs.

Dual model				
Point Cloud	Avg. Bpp on MPEG 8i	Encoding time (s)	Decoding time (s)	
			Total	Network
Loot10	0.56	1.71	14.0	8.1
Redandblack10	0.67	1.57	12.9	7.5
Boxer9	0.54	0.60	4.6	2.9
Boxer10	0.53	2.08	17.1	10.1
Thaidancer	0.60	0.58	4.6	2.8
Thaidancer10	0.59	2.02	17.0	10.0
Average	0.58	1.43	11.7	6.9

Table 16. Dual model, context window length $n = 2048$, group count $g = 8$, training for 20 epochs.

4.5. Results of Window Length Ablation Study

We use dual model, set group count $g = 8$, and change context window length $n \in$

{128, 256, 512, 1024, 2048, 4096}. The complete results of each model is shown in Tab. 17 to 21.

Context Window Ablation Test $n = 128$				
Point Cloud	Avg. Bpp on MPEG 8i	Encoding time (s)	Decoding time (s)	
			Total	Network
Loot10	0.64	12.9	117.4	100.3
Redandblack10	0.75	11.8	106.0	90.6
Boxer9	0.62	4.2	38.1	32.6
Boxer10	0.60	16.1	148.3	126.3
Thaidancer	0.68	4.0	37.1	31.8
Thaidancer10	0.67	15.8	146.1	124.2
Average	0.66	10.8	98.8	84.3

Table 17. Dual model, context window length $n = 128$, group count $g = 8$, training for 20 epochs.

Context Window Ablation Test $n = 256$				
Point Cloud	Avg. Bpp on MPEG 8i	Encoding time (s)	Decoding time (s)	
			Total	Network
Loot10	0.63	6.54	64.5	52.1
Redandblack10	0.75	6.04	60.1	48.2
Boxer9	0.62	2.11	21.3	17.1
Boxer10	0.59	8.30	82.6	66.1
Thaidancer	0.68	2.12	20.7	16.6
Thaidancer10	0.66	8.10	80.5	64.7
Average	0.66	5.54	55.0	44.1

Table 18. Dual model, context window length $n = 256$, group count $g = 8$, training for 20 epochs.

Context Window Ablation Test $n = 512$				
Point Cloud	Avg. Bpp on MPEG 8i	Encoding time (s)	Decoding time (s)	
			Total	Network
Loot10	0.59	3.19	35.5	26.6
Redandblack10	0.70	2.91	32.8	24.5
Boxer9	0.57	1.06	12.0	8.9
Boxer10	0.55	3.97	43.6	33.2
Thaidancer	0.63	1.04	11.2	8.4
Thaidancer10	0.62	3.93	44.0	33.1
Average	0.61	2.68	29.9	22.5

Table 19. Dual model, context window length $n = 512$, group count $g = 8$, training for 20 epochs.

4.6. Results of Group Count Ablation Study

We use dual model, set context window length $n = 2048$, and change group count $g \in \{2, 4, 8, 16, 32\}$. The complete results of each model is shown in Tab. 22 to 26.

Context Window Ablation Test $n = 1024$				
Point Cloud	Avg. Bpp on MPEG 8i	Encoding time (s)	Decoding time (s)	
			Total	Network
Loot10	0.57	1.70	19.3	13.0
Redandblack10	0.68	1.57	17.9	12.0
Boxer9	0.55	0.58	6.2	4.3
Boxer10	0.53	2.17	25.1	16.5
Thaidancer	0.61	0.58	6.2	4.2
Thaidancer10	0.60	2.14	23.5	15.8
Average	0.59	1.46	16.4	11.0

Table 20. Dual model, context window length $n = 1024$, group count $g = 8$, training for 20 epochs.

Context Window Ablation Test $n = 2048$				
Point Cloud	Avg. Bpp on MPEG 8i	Encoding time (s)	Decoding time (s)	
			Total	Network
Loot10	0.56	1.71	14.0	8.1
Redandblack10	0.67	1.57	12.9	7.5
Boxer9	0.54	0.60	4.6	2.9
Boxer10	0.53	2.08	17.1	10.1
Thaidancer	0.60	0.58	4.6	2.8
Thaidancer10	0.59	2.02	17.0	10.0
Average	0.58	1.43	11.7	6.9

Table 21. Dual model, context window length $n = 2048$, group count $g = 8$, training for 20 epochs.

Group Count Ablation Test $g = 2$				
Point Cloud	Avg. Bpp on MPEG 8i	Encoding time (s)	Decoding time (s)	
			Total	Network
Loot10	0.63	1.67	9.3	3.0
Redandblack10	0.74	1.54	8.6	2.8
Boxer9	0.62	0.60	3.1	1.0
Boxer10	0.59	2.10	11.8	3.8
Thaidancer	0.69	0.58	3.0	1.0
Thaidancer10	0.66	1.78	11.7	3.7
Average	0.66	1.38	7.9	2.6

Table 22. Dual model, context window length $n = 2048$, group count $g = 2$, training for 20 epochs.

Group Count Ablation Test $g = 4$				
Point Cloud	Avg. Bpp on MPEG 8i	Encoding time (s)	Decoding time (s)	
			Total	Network
Loot10	0.59	1.57	10.2	4.2
Redandblack10	0.70	1.46	9.5	3.9
Boxer9	0.57	0.57	3.5	1.5
Boxer10	0.55	1.98	13.1	5.3
Thaidancer	0.64	0.55	3.4	1.5
Thaidancer10	0.62	1.66	12.8	5.2
Average	0.61	1.30	8.8	3.6

Table 23. Dual model, context window length $n = 2048$, group count $g = 4$, training for 20 epochs.

Group Count Ablation Test $g = 8$				
Point Cloud	Avg. Bpp on MPEG 8i	Encoding time (s)	Decoding time (s)	
			Total	Network
Loot10	0.56	1.71	14.0	8.1
Redandblack10	0.67	1.57	12.9	7.5
Boxer9	0.54	0.60	4.6	2.9
Boxer10	0.53	2.08	17.1	10.1
Thaidancer	0.60	0.58	4.6	2.8
Thaidancer10	0.59	2.02	17.0	10.0
Average	0.58	1.43	11.7	6.9

Table 24. Dual model, context window length $n = 2048$, group count $g = 8$, training for 20 epochs.

Group Count Ablation Test $g = 16$				
Point Cloud	Avg. Bpp on MPEG 8i	Encoding time (s)	Decoding time (s)	
			Total	Network
Loot10	0.55	1.60	22.8	16.0
Redandblack10	0.66	1.48	20.8	14.8
Boxer9	0.53	0.58	7.8	5.6
Boxer10	0.52	1.37	28.5	20.2
Thaidancer	0.59	0.56	7.7	5.5
Thaidancer10	0.58	1.96	27.7	19.7
Average	0.57	1.26	19.2	13.6

Table 25. Dual model, context window length $n = 2048$, group count $g = 16$, training for 20 epochs.

Group Count Ablation Test $g = 32$				
Point Cloud	Avg. Bpp on MPEG 8i	Encoding time (s)	Decoding time (s)	
			Total	Network
Loot10	0.55	1.60	39.1	31.2
Redandblack10	0.66	1.49	36.2	28.9
Boxer9	0.53	0.58	13.6	10.9
Boxer10	0.51	2.02	49.1	39.3
Thaidancer	0.58	0.56	13.1	10.6
Thaidancer10	0.57	1.97	48.6	38.6
Average	0.57	1.37	33.3	26.6

Table 26. Dual model, context window length $n = 2048$, group count $g = 32$, training for 20 epochs.

References

- [1] Thomas M Cover and Joy A Thomas. Elements of information theory 2nd edition (wiley series in telecommunications and signal processing). *Acessado em*, 2006.
- [2] Yu Feng, Shaoshan Liu, and Yuhao Zhu. Real-time spatio-temporal lidar point cloud compression. In *2020 IEEE/RSJ international conference on intelligent robots and systems (IROS)*, pages 10766–10773. IEEE, 2020.
- [3] Chunyang Fu, Ge Li, Rui Song, Wei Gao, and Shan Liu. Octtention: Octree-based large-scale contexts model for point cloud compression. *arXiv preprint arXiv:2202.06028*, 2022.
- [4] Yun He, Xinlin Ren, Danhang Tang, Yinda Zhang, Xiangyang Xue, and Yanwei Fu. Density-preserving deep point cloud compression. In *Proceedings of the IEEE/CVF Con-*

- ference on Computer Vision and Pattern Recognition, pages 2333–2342, 2022.
- [5] Fei Huang, Tianhua Tao, Hao Zhou, Lei Li, and Minlie Huang. On the learning of non-autoregressive transformers. In Kamalika Chaudhuri, Stefanie Jegelka, Le Song, Csaba Szepesvari, Gang Niu, and Sivan Sabato, editors, *Proceedings of the 39th International Conference on Machine Learning*, volume 162 of *Proceedings of Machine Learning Research*, pages 9356–9376. PMLR, 17–23 Jul 2022.
 - [6] Tianxin Huang and Yong Liu. 3d point cloud geometry compression on deep learning. In *Proceedings of the 27th ACM international conference on multimedia*, pages 890–898, 2019.
 - [7] Zujie Liang and Fan Liang. Transpcc: Towards deep point cloud compression via transformers. 2022.
 - [8] MPEG. <https://github.com/MPEGGroup/mpeg-pcc-tmc13>, 2021.
 - [9] Dat Thanh Nguyen, Maurice Quach, Giuseppe Valenzise, and Pierre Duhamel. Learning-based lossless compression of 3d point cloud geometry. In *ICASSP 2021-2021 IEEE International Conference on Acoustics, Speech and Signal Processing (ICASSP)*, pages 4220–4224. IEEE, 2021.
 - [10] Dat Thanh Nguyen, Maurice Quach, Giuseppe Valenzise, and Pierre Duhamel. Lossless coding of point cloud geometry using a deep generative model. *IEEE Transactions on Circuits and Systems for Video Technology*, 31(12):4617–4629, 2021.
 - [11] Dat Thanh Nguyen, Maurice Quach, Giuseppe Valenzise, and Pierre Duhamel. Multiscale deep context modeling for lossless point cloud geometry compression. In *2021 IEEE International Conference on Multimedia & Expo Workshops (ICMEW)*, pages 1–6. IEEE, 2021.
 - [12] Maurice Quach, Giuseppe Valenzise, and Frederic Dufaux. Learning convolutional transforms for lossy point cloud geometry compression. In *2019 IEEE international conference on image processing (ICIP)*, pages 4320–4324. IEEE, 2019.
 - [13] Maurice Quach, Giuseppe Valenzise, and Frederic Dufaux. Improved deep point cloud geometry compression. In *2020 IEEE 22nd International Workshop on Multimedia Signal Processing (MMSP)*, pages 1–6. IEEE, 2020.
 - [14] Zizheng Que, Guo Lu, and Dong Xu. Voxelcontext-net: An octree based framework for point cloud compression. In *Proceedings of the IEEE/CVF Conference on Computer Vision and Pattern Recognition*, pages 6042–6051, 2021.
 - [15] Xuebin Sun, Han Ma, Yuxiang Sun, and Ming Liu. A novel point cloud compression algorithm based on clustering. *IEEE Robotics and Automation Letters*, 4(2):2132–2139, 2019.
 - [16] Chenxi Tu, Eijiro Takeuchi, Alexander Carballo, and Kazuya Takeda. Point cloud compression for 3d lidar sensor using recurrent neural network with residual blocks. In *2019 International Conference on Robotics and Automation (ICRA)*, pages 3274–3280. IEEE, 2019.
 - [17] Jianqiang Wang, Dandan Ding, Zhu Li, Xiaoxing Feng, Chuntong Cao, and Zhan Ma. Sparse tensor-based multi-scale representation for point cloud geometry compression. *arXiv preprint arXiv:2111.10633*, 2021.
 - [18] Jianqiang Wang, Dandan Ding, Zhu Li, and Zhan Ma. Multi-scale point cloud geometry compression. In *2021 Data Compression Conference (DCC)*, pages 73–82. IEEE, 2021.
 - [19] Kang You and Pan Gao. Patch-based deep autoencoder for point cloud geometry compression. In *ACM Multimedia Asia*, pages 1–7. 2021.
 - [20] Lili Zhao, Kai-Kuang Ma, Zhili Liu, Qian Yin, and Jianwen Chen. Real-time scene-aware lidar point cloud compression using semantic prior representation. *IEEE Transactions on Circuits and Systems for Video Technology*, 2022.